An endoplasmic reticulum–localized cytochrome b_5 regulates high-affinity K^+ transport in response to salt stress in rice

Tengzhao Song[a], Yiyuan Shi[a], Like Shen[a], Chengjuan Cao[a], Yue Shen[a], Wen Jing[a], Quanxiang Tian[a], Feng Lin[a], Wenyu Li[a,1], and Wenhua Zhang[a,1]

[a]College of Life Sciences, State Key Laboratory of Crop Genetics and Germplasm Enhancement, Nanjing Agricultural University, Nanjing 210095, China

Edited by Julian Schroeder, University of California San Diego, La Jolla, CA; received August 4, 2021; accepted November 1, 2021

Potassium (K^+) is an essential element for growth and development in both animals and plants, while high levels of environmental sodium (Na^+) represent a threat to most plants. The uptake of K^+ from high-saline environments is an essential mechanism to maintain intracellular K^+/Na^+ homeostasis, which can help reduce toxicity caused by Na^+ accumulation, thereby improving the salt tolerance of plants. However, the mechanisms and regulation of K^+-uptake during salt stress remain poorly understood. In this study, we identified an endoplasmic reticulum–localized cytochrome b_5 (OsCYB5-2) that interacted with a high-affinity K^+ transporter (OsHAK21) at the plasma membrane. The association of OsCYB5-2 with the OsHAK21 transporter caused an increase in transporter activity by enhancing the apparent affinity for K^+-binding but not Na^+-binding. Heme binding to OsCYB5-2 was essential for the regulation of OsHAK21. High salinity directly triggered the OsHAK21–OsCYB5-2 interaction, promoting OsHAK21-mediated K^+-uptake and restricting Na^+ entry into cells; this maintained intracellular K^+/Na^+ homeostasis in rice cells. Finally, overexpression of *OsCYB5-2* increased OsHAK21-mediated K^+ transport and improved salt tolerance in rice seedlings. This study revealed a posttranslational regulatory mechanism for HAK transporter activity mediated by a cytochrome b_5 and highlighted the coordinated action of two proteins to perceive Na^+ in response to salt stress.

rice | HAK transporter | cytochrome b5 | ion homeostasis | salt tolerance

Soil salinity is a major limiting factor for plant growth and crop production. Salinity tolerance in plants is conferred by maintaining an optimal cytosolic potassium/sodium (K^+/Na^+) ratio rather than the absolute Na^+ concentration (1, 2). During salt stress, high-Na^+ levels disrupt K^+/Na^+ homeostasis by reducing K^+ uptake and increasing K^+ efflux (3, 4). Increasing K^+ uptake from high-Na^+ environments can effectively improve plant salt tolerance by maintaining K^+/Na^+ homeostasis (5–8).

The absorption of K^+ in roots and the distribution of K^+ throughout the plant are primarily regulated by K^+ channels and transporters (9). The K^+ transporter/high-affinity K^+ transporter/K^+ uptake protein (KT/HAK/KUP) family is one of the principal K^+ acquisition systems in plants (10). They are involved in processes such as K^+ uptake from the soil, K^+ translocation, water movement regulation, and developmental processes (11, 12). Kinetic analyses of plant roots of Rb^+ (as a K^+ tracer) involving comparison of wild-type (WT) and *AtHAK5* knockout mutant have revealed that AtHAK5 functions in K^+ deprivation–induced, high-affinity K^+ uptake in *Arabidopsis* roots (13, 14). In monocot rice, some HAKs, such as OsHAK1, OsHAK5, OsHAK16, and OsHAK21, play essential roles in specific tissues and/or cells when plants are subjected to salt stress (8, 15–18). For example, *OsHAK21* transcription is strongly up-regulated in roots following salt stress, and knockdown of this gene leads to less K^+ and more Na^+ accumulation in plants. Furthermore, *OsHAK21* expression can be beneficial for an *Arabidopsis athak5* mutant defective in K^+-uptake in low-K^+ environments, suggesting that OsHAK21 has HAK transport activity (8). This gene is also involved in seed germination and seedling establishment under salinity stress (17). These results demonstrate the involvement of OsHAK21 in K^+ uptake and salt tolerance. In heterologous oocyte systems, HAK currents are regulated by the *Arabidopsis* Ca^{2+} sensor kinase pairs AtCBL1/AtCIPK23 and AtCBL9/AtCIPK23 (11, 19). More recently, the requirement for Ser35 phosphorylation of AtCIPK23 has been proposed for the activity of AtHAK5 under low-K^+ conditions (20). However, the regulatory mechanisms of HAKs during salt stress in plants remain unclear.

Plant cytochrome b_5 (CYB5s) are hemoproteins anchored to the endoplasmic reticulum (ER) or chloroplast envelope via C-terminal hydrophobic domains, and their hydrophilic N-terminal domains protrude into the cytosol (21–24). Similar to those in mammals and yeasts, plant CYB5s also commonly serve as essential electron shuttle intermediates for biosynthetic reactions, such as lipid, steroid, and lignin biosynthesis (24–27). CYB5 proteins physically associate with AtRTE1 and AtSUT4 to mediate the ethylene response and sucrose transport, respectively (28–30). Here, we found that the ER-localized OsCYB5-2 protein interacts with OsHAK21. Our biochemical analyses indicated that the OsCYB5-2–OsHAK21 interaction enhances the apparent affinity of OsHAK21 for K^+-binding and improves K^+ transport activity. We provide further genetic evidence

Significance

High-affinity K^+ (HAK) transporter-mediated K^+ uptake has an important role when plants are subjected to stresses. This work identifies a mechanism of HAK regulation. The affinity of HAK at the plasma membrane for K^+ depends on the binding of a cytochrome (CYB5) protein at the endoplasmic reticulum. This improves K^+ uptake and the ability of plants to survive under saline conditions. The HAK–CYB5 interaction not only constitutes a mechanism of HAK regulation but also reflects interorganelle communication mediated by functional protein interactions under conditions of stress.

Author contributions: T.S., W.L., and W.Z. designed research; T.S., Y. Shi, L.S., C.C., Y. Shen, W.J., Q.T., and W.L. performed research; T.S., Y. Shi, L.S., C.C., Y. Shen, W.J., Q.T., and W.L. analyzed data; T.S., F.L., W.L., and W.Z. wrote the paper; and F.L. and W.Z. supervised the research.

The authors declare no competing interest.

This article is a PNAS Direct Submission.

[1]To whom correspondence may be addressed. Email: liwenyu0708@163.com or whzhang@njau.edu.cn.

This article contains supporting information online at http://www.pnas.org/lookup/suppl/doi:10.1073/pnas.2114347118/-/DCSupplemental.

Published December 7, 2021.

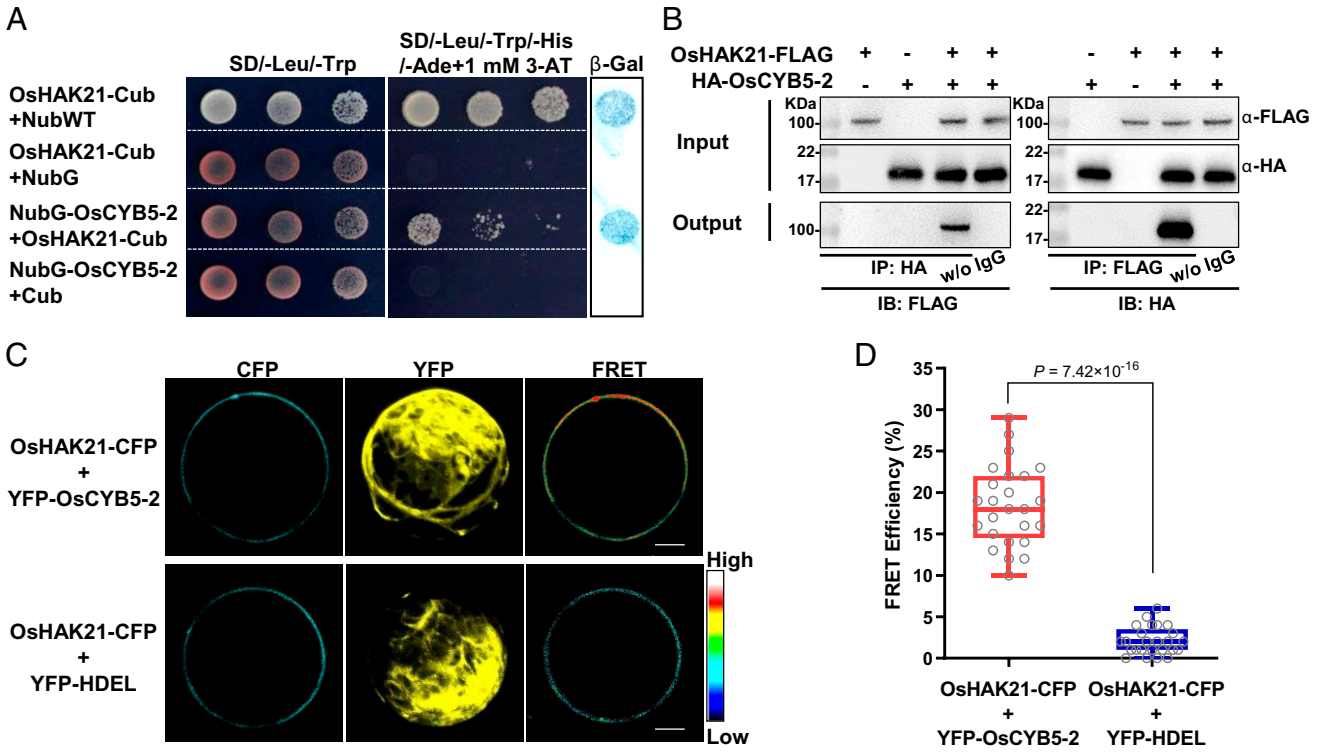

Fig. 1. The Interaction between OsHAK21 and OsCYB5-2. (*A*) OsHAK21 interacts with OsCYB5-2 in yeast split-ubiquitin system. The 1:10 serial dilutions of yeast cells were spotted on control medium (*Left*) or selective medium (*Middle*). The same set of yeast transformants were assayed for β-gal activities developed on filter paper (*Right*). (*B*) Co-IP analysis for OsHAK21 and OsCYB5-2 interaction in agrobacterium-infiltrated tobacco leaves. OsHAK21-FLAG and HA-OsCYB5-2 were coexpressed as the indicated combinations (*Top*). "-" represents vector alone. Proteins (*Left*) were immunoprecipitated with anti-HA antibody (IP: HA) and detected with anti-FLAG antibody (IB: FLAG). Proteins (*Right*) were immunoprecipitated with anti-FLAG antibody (IP: FLAG) and detected with anti-HA antibody (IB: HA). Beads incubating proteins without (w/o) IgG are negative controls. (*C*) Rice protoplasts coexpressing OsHAK21-CFP and YFP-OsCYB5-2 were examined by confocal laser scanning microscopy. YFP-HDEL is a negative control of ER marker protein. (Scale bar, 20 μm.) (*D*) Quantitative FRET analysis for the interaction between OsHAK21-CFP and YFP-OsCYB5-2. The box plots depict the mean FRET efficiency from one experiment with $n = 25$ protoplasts. The boxes indicate the first and third quartiles, and the whiskers indicate the minimum to maximum values. The lines within the boxes indicate the median values. Statistically significant differences were determined by the two-tailed Student's *t* test. Three independent experiments were repeated with similar results.

demonstrating that OsCYB5-2 regulates OsHAK21-mediated K^+ uptake, thereby counteracting Na^+ toxicity in rice cells.

Results

High-Affinity K^+ Transporter OsHAK21 Interacts with an ER-Localized OsCYB5. OsHAK21 has been identified as a functional K^+ transporter that maintains K^+/Na^+ homeostasis in response to salt stress (8). To further elucidate the posttranslational regulatory mechanisms for OsHAK21, the yeast split-ubiquitin system was employed to screen for potential proteins that interact with OsHAK21 (31). Of 2.3×10^8 transformants, we obtained 21 putative interactors, of which two CYB5-like heme/steroid binding domain–containing proteins (LOC_Os12g12170 [OsCYB5-1] and LOC_Os10g37420 [OsCYB5-2]) were identified (*SI Appendix*, Fig. S1). There are 14 members of the CYB5 family in rice and six members in *Arabidopsis* (SI Appendix, Fig. S2*A*) (26); we collectively named this family OsCYB5-n (n represents 1 through 14) (*SI Appendix*, Fig. S2*A*). OsCYB5-n were predicted to contain conserved structural characteristics: an N-terminal cytosolic heme-binding domain, a C-terminal transmembrane domain that anchors the protein to the ER or mitochondria/chloroplast, and a short luminal tail (*SI Appendix*, Fig. S2*B*) (21, 22). According to the β-glucuronidase (GUS) staining results, OsCYB5-1 showed weak transcription in young leaf. Roots of transgenic seedlings were not stained, while OsCYB5-2 expression was ubiquitous and strong in the tested tissues (*SI Appendix*, Fig. S3). We selected OsCYB5-2 as a putative OsHAK21 interactive partner for further analysis.

The interaction of OsHAK21–OsCYB5-2 was first determined using a yeast split-ubiquitin system (Fig. 1*A*). Yeast strains expressing the N-terminal half of yeast ubiquitin (NubWT) combined with the C-terminal half of yeast ubiquitin (Cub) fused with OsHAK21 (OsHAK21-Cub) were used as a positive control; yeast strains expressing Nub (G, mutant) combined with OsHAK21-Cub were used as a negative control. Yeast growth was observed for protein couples of positive control and OsHAK21-Cub/NubG-OsCYB5-2, suggesting that OsHAK21 and OsCYB5-2 physically interact. The results matched those obtained from a β-galactosidase (β-Gal) activity assay (Fig. 1*A*). To confirm the OsHAK21 and OsCYB5-2 interaction, C-terminally FLAG-tagged OsHAK21 and N-terminally hemagglutinin (HA)-tagged OsCYB5-2 were coexpressed in tobacco leaves, followed by coimmunoprecipitation (co-IP). The results showed that OsHAK21-FLAG and HA-OsCYB5-2 immunoprecipitated together (Fig. 1*B*).

To further investigate the interaction between OsHAK21 and OsCYB5-2 in plant cells, we first determined their cellular location. OsCYB5-2 was fused with green fluorescence protein (GFP) to produce GFP-OsCYB5-2; GFP-OsCYB5-2 showed a reticular morphology, which overlapped with the red fluorescence from mCherry-fused ER marker HDEL (*SI Appendix*, Fig. S4), indicating that OsCYB5-2 localized to the ER in plant cells. In previous work, OsHAK21 was shown to localize to the

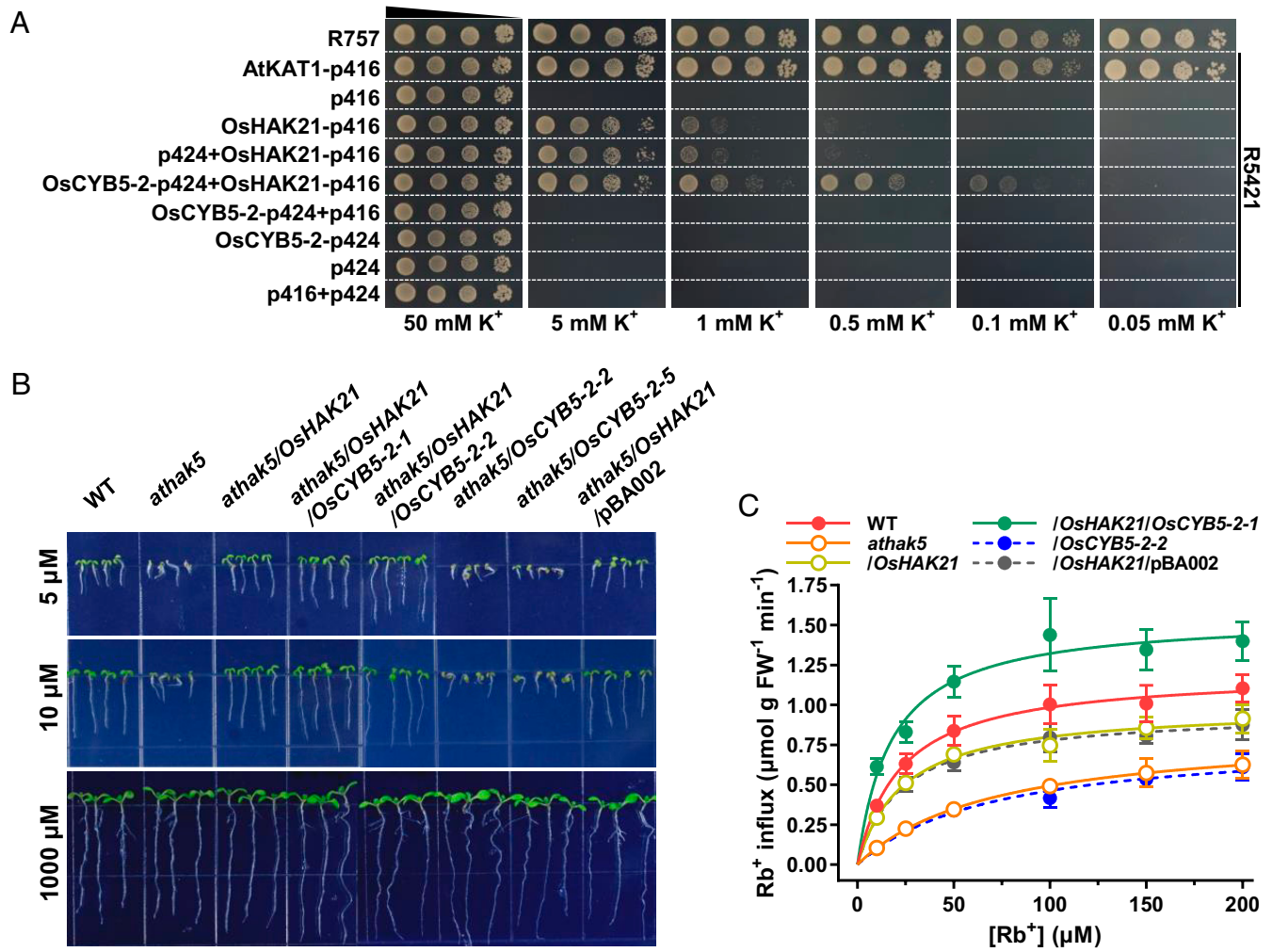

Fig. 2. OsCYB5-2 increases K^+ transport activity of OsHAK21 in yeasts and plants. (*A*) OsCYB5-2 enhances the growth of K^+-uptake-deficient yeast mutant R5421 expressing OsHAK21 on low-K^+ AP medium. The WT yeast strain R757 was used as a positive control. AtKAT1, a K^+ channel from *Arabidopsis*, was transformed into R5421 as a positive control. *OsHAK21* and *OsCYB5-2* were constructed into p416 and p424 vector. respectively. The 1:10 serial dilutions (as black triangle) of yeast cells were spotted on the AP medium. (*B*) Phenotypes of *Arabidopsis* transgenic lines expressing *OsCYB5-2* and *OsHAK21* in *athak5* mutant. The seedlings were grown for 12 d on the medium containing K^+ as the concentrations indicated. (*C*) Kinetics of Rb^+ uptake in roots of WT, *athah5*, and *Arabidopsis* transgenic lines as described in *B* after 7 d of K^+ starvation. The data are shown as means ± SD from $n = 5$ seedlings. Curves represent results of fitting Michaelis–Menten equation. FW, Fresh weight.

PM (8). We then applied a Förster resonance energy transfer (FRET) assay using OsCYB5-2 fused to yellow fluorescent protein (YFP-OsCYB5-2) and OsHAK21 fused to cyan fluorescent protein (OsHAK21-CFP). When YFP-OsCYB5-2 and OsHAK21-CFP were coexpressed in rice protoplasts, they produced high levels of FRET, which were 4.5-fold higher than the FRET generated during OsHAK21-CFP and YFP-HDEL coexpression (Fig. 1 *C* and *D*). Taken together, the results suggest specific binding between OsHAK21 and OsCYB5-2 in vivo.

In addition, the transgenic plants carrying *OsCYB5-2* promoter::GUS showed that *OsCYB5-2* was ubiquitously expressed in all tissues (*SI Appendix*, Fig. S3), and a similar pattern was found for *OsHAK21* (8). A cross-section of GUS-stained roots showed strong signals in most cell types, consistent with the expression of *OsHAK21* in xylem parenchyma and endodermal cells (*SI Appendix*, Fig. S3*E*) (8). Strong GUS activity driven by the *OsCYB5-2* promoter was detected in germinating embryos (*SI Appendix*, Fig. S3 *I* and *J*), similar to *OsHAK21* expression during germination (17). These results suggest that the expression patterns of *OsCYB5-2* and *OsHAK21* are spatially and temporally similar, which increases the likelihood of interaction between OsHAK21 and OsCYB5-2 in rice.

OsCYB5-2 Enhances K^+ Transport Activity of OsHAK21. To explore the biological significance of the interaction between OsCYB5-2 and OsHAK21, the K^+-uptake–defective auxotrophic yeast mutant strain R5421 (*trk1Δ* and *trk2Δ*) was transformed with OsCYB5-2, OsHAK21, or both simultaneously (32, 33). OsHAK21 expression improved yeast growth under as low as 1 mM K^+, suggesting that OsHAK21 exhibits K^+-uptake activity in yeast cells. OsHAK21 activity was, however, weaker than that of the *Arabidopsis* K^+ transporter AtKAT1 (34) and the WT yeast transporter R757. Coexpression of OsCYB5-2 and OsHAK21 further improved growth in yeast transformants under lower K^+ concentrations (≤0.5 mM). OsCYB5-2 expression alone did not improve yeast growth (Fig. 2*A*). In a kinetic study of K^+ depletion, yeast cells coexpressing OsCYB5-2 and OsHAK21 showed more rapid depletion of external K^+ than cells expressing OsHAK21 alone at micromolar K^+ concentrations, while no obvious depletion was observed in cells expressing OsCYB5-2 (*SI Appendix*, Fig. S5*A*). The results suggest that OsCYB5-2 expression enhanced the K^+ transport activity of OsHAK21 in yeast cells.

We then examined how OsCYB5-2 expression affects OsHAK21 activity in plants. The overexpression of *OsHAK21* complemented *athak5* growth in low K^+ (5 or 10 μM), suggesting that

OsHAK21 improved K^+ uptake in *Arabidopsis* (Fig. 2*B* and *SI Appendix*, Fig. S5 *B* and *C*) (8, 35). The simultaneous expression of *OsHAK21* and *OsCYB5-2* in the *athak5* mutant (*athak5*/*OsHAK21*/*OsCYB5-2*) improved plant growth even further, exhibiting increased root length and fresh weight compared to the *athak5*/*OsHAK21* and WT plants. No significant changes in growth were observed in lines overexpressing *OsCYB5-2* (Fig. 2*B* and *SI Appendix*, Fig. S5 *B* and *C*).

Direct measurements of K^+-tracer Rb^+ transport kinetics in plants revealed that overexpression of *OsHAK21* complemented the impairment of HAK uptake in *athak5* (Fig. 2*C*). Coexpression of *OsCYB5-2* with *OsHAK21* improved K^+ uptake in plants compared to that of *OsHAK21* only by increasing V_{max} and decreasing K_m. By contrast, overexpression of *OsCYB5-2* only did not change the kinetic parameters for K^+ uptake (*SI Appendix*, Fig. S5*D*). Together, these results indicate that OsCYB5-2 can increase OsHAK21 activity, thereby indirectly promoting K^+ uptake in plants.

OsCYB5-2 and OsHAK21 Interaction Improves Salt Tolerance in Rice. To test our hypothesis that interaction of OsCYB5-2 and OsHAK21 improves salt-stress tolerance in rice, we first expressed OsCYB5-2 and OsHAK21 in a heterologous yeast system to examine its effect on growth at various NaCl concentrations. Yeast transformants expressing OsHAK21 or OsCYB5-2 could not grow vigorously at all NaCl concentrations (100 to 400 mM) tested. The combined expression of OsHAK21 and OsCYB5-2 significantly improved yeast growth, even at high (300 mM)-NaCl concentrations (*SI Appendix*, Fig. S6*A*). The improvement of salt tolerance by the combined overexpression of *OsHAK21* and *OsCYB5-2* was confirmed in transgenic *Arabidopsis* plants (*SI Appendix*, Fig. S6 *B* and *C*).

The interaction between OsHAK21 and OsCYB5-2 was then investigated in rice plants. *OsCYB5-2* expression increased under salt stress, similar to that of *OsHAK21* (*SI Appendix*, Fig. S7) (8). The *OsCYB5-2*-overexpressing rice plants with WT background (WT/*OsCYB5-2-OE*) showed high tolerance to salt stress and significantly higher fresh weight and chlorophyll content relative to WT plants transformed with empty vector (WT/vector) (Fig. 3 *A*–*C*). Moreover, when *OsCYB5-2* was overexpressed in the *oshak21* mutant background (8), no mitigating effects were observed (Fig. 3 *A*–*C*), suggesting that the function of OsCYB5-2 is OsHAK21 dependent.

To investigate whether the OsHAK21–OsCYB5-2 interaction regulates K^+ and Na^+ homeostasis in rice plants, their contents in the transgenic plants were analyzed. Under control conditions, no significant difference in Na^+ (or K^+) content or ratio was observed among the transgenic lines (Fig. 3 *D*–*F* and *SI Appendix*, Fig. S8). Following NaCl treatment for 12 d, WT/*OsCYB5-2-OE* plants accumulated the lowest Na^+ and highest K^+ among the transgenic rice lines in both shoots and roots (Fig. 3 *D* and *E* and *SI Appendix*, Fig. S8 *A* and *B*), which resulted in the lowest Na^+/K^+ ratios (Fig. 3*F* and *SI Appendix*, Fig. S8*C*). Moreover, overexpression of *OsCYB5-2* increased K^+ net uptake and decreased Na^+ net uptake under NaCl stress conditions (Fig. 3 *G* and *H*). Taken together, these results indicate that OsCYB5-2 increases OsHAK21 activity and promotes K^+ uptake, which is essential for the maintenance of K^+/Na^+ homeostasis and salt tolerance in rice.

Salt Stress Triggers the OsHAK21–OsCYB5-2 Interaction. We investigated whether and how salt stress affects the interaction between OsHAK21 and OsCYB5-2. We first used the yeast split-ubiquitin system to quantify the OsHAK21–OsCYB5-2 interaction (estimated based on the β-Gal activity; *SI Appendix*, Fig. S9*A*) and found that high Na^+ significantly enhanced β-Gal activity in a dose- and time-dependent manner (*SI Appendix*, Fig. S9 *B* and *N*). We used OsHAK21-Cub+NubWT, which shows high β-Gal activity, as a control and found that the activity did not change at different concentrations of NaCl (0 to 400 mM) over 4 h. Another control, OsHAK21-Cub+NubG, also did not change according to the concentration of NaCl. The results suggest that the increase in β-Gal activity is specific for OsHAK21 and OsCYB5-2 binding. Importantly, the interaction did not vary according to the isotonic concentrations of K^+ and mannitol or K^+ deficiency (*SI Appendix*, Fig. S9). The results suggest that the increase in the degree of OsHAK21–OsCYB5-2 interaction is a specific response to high-Na^+ stress.

To examine the OsHAK21–OsCYB5-2 interaction in rice cells, we developed constructs that enable coexpression of multiple chimeric fluorescent fusion proteins in suspension cells (Fig. 4*A* and *SI Appendix*, Fig. S10 *A* and *B*) (36). The vectors facilitate fusion of the gene of interest with 3×FLAG-tagged CFP (FC) and HA-tagged YFP (YH), thus enabling detection of protein interactions using FRET and co-IP analysis (Fig. 4 *A*–*D*). We coexpressed OsHAK21-FC with YH-OsCYB5-2 in rice suspension cells of the *oshak21* background. Transformant protoplasts were isolated to examine the OsHAK21–OsCYB5-2 interaction via FRET (Fig. 4 *A* and *B*). The resulting FRET efficiency, indicative of the OsHAK21–OsCYB5-2 interaction, was determined by dividing the emission intensity of FRET by the emission intensity of CFP (FRET/CFP) at predefined time points (37). The FRET efficiency (FRET/CFP) is proportional to the intensity of the two-protein interaction. Protoplasts coexpressing OsHAK21-FC and YH-OsCYB5-2 exhibited an increase in FRET efficiency following treatment with 100 mM NaCl but not with isotonic concentrations of mannitol (200 mM), indicating that the interaction between the two proteins was enhanced under salt stress (Fig. 4 *B* and *C*). NaCl treatment did not increase the interaction between another pair of proteins, AtVST1 in the peripheral PM and AtSRC2 in the ER (*SI Appendix*, Fig. S10 *A*–*D*) (38); the interaction of these proteins has been shown to regulate stomatal development signaling (38). FRET efficiency changed in response to the addition of the bacterial flagellar peptide (flg22) to the protoplast expressing the flg22 receptor AtFLS2 and a receptor-like kinase (AtNIK1 or AtBIK1) (39, 40). However, the AtFLS2–AtNIK1/AtBIK1 interaction were not affected by NaCl or mannitol treatment (*SI Appendix*, Fig. S10 *C*–*E*). These results show that high-salt conditions specifically induce the interaction of OsHAK21 and OsCYB5-2 through ionic stress.

Suspension cells coexpressing OsHAK21-FC and YH-OsCYB5-2 were incubated in 100 mM NaCl, and the YH-OsCYB5-2/OsHAK21-FC interaction was quantified by performing co-IP over a time course of 60 min. The expression levels of OsHAK21-FC and YH-OsCYB5-2 did not change from 0 to 60 min of NaCl (0 or 100 mM) treatment. YH-OsCYB5-2/OsHAK21-FC binding increased following treatment with 100 mM NaCl, but binding did not change with 0 mM NaCl treatment (Fig. 4*D* and *SI Appendix*, Fig. S10*F*), suggesting that salt stress induces OsCYB5-2 binding to OsHAK21.

The K^+ and Na^+ contents were determined in rice suspension cells (*oshak21* background) expressing either *OsHAK21* (vector *iii*), *OsCYB5-2* (vector *iv*), or both (vector *ii*) (Fig. 4*A*); expression was confirmed by transcription analysis (Fig. 4 *F* and *G*, *Insets*). Cells coexpressing *OsCYB5-2* and *OsHAK21* displayed increased K^+ content and reduced Na^+ accumulation at 90 to 120 min relative to transformants expressing *OsHAK21* only incubated in salt (Fig. 4 *E*–*G*). The results suggest that salt stimulation triggers OsCYB5-2 binding to OsHAK21, which then mediates K^+/Na^+ homeostasis in cells; this is consistent with the genetic and physiological results (Fig. 3).

Leucine 128 in OsHAK21 Is a Key Residue for OsCYB5-2 Binding. To identify the region of the OsHAK21 protein involved in OsCYB5-2 binding, serial deletion mutants of OsHAK21 were

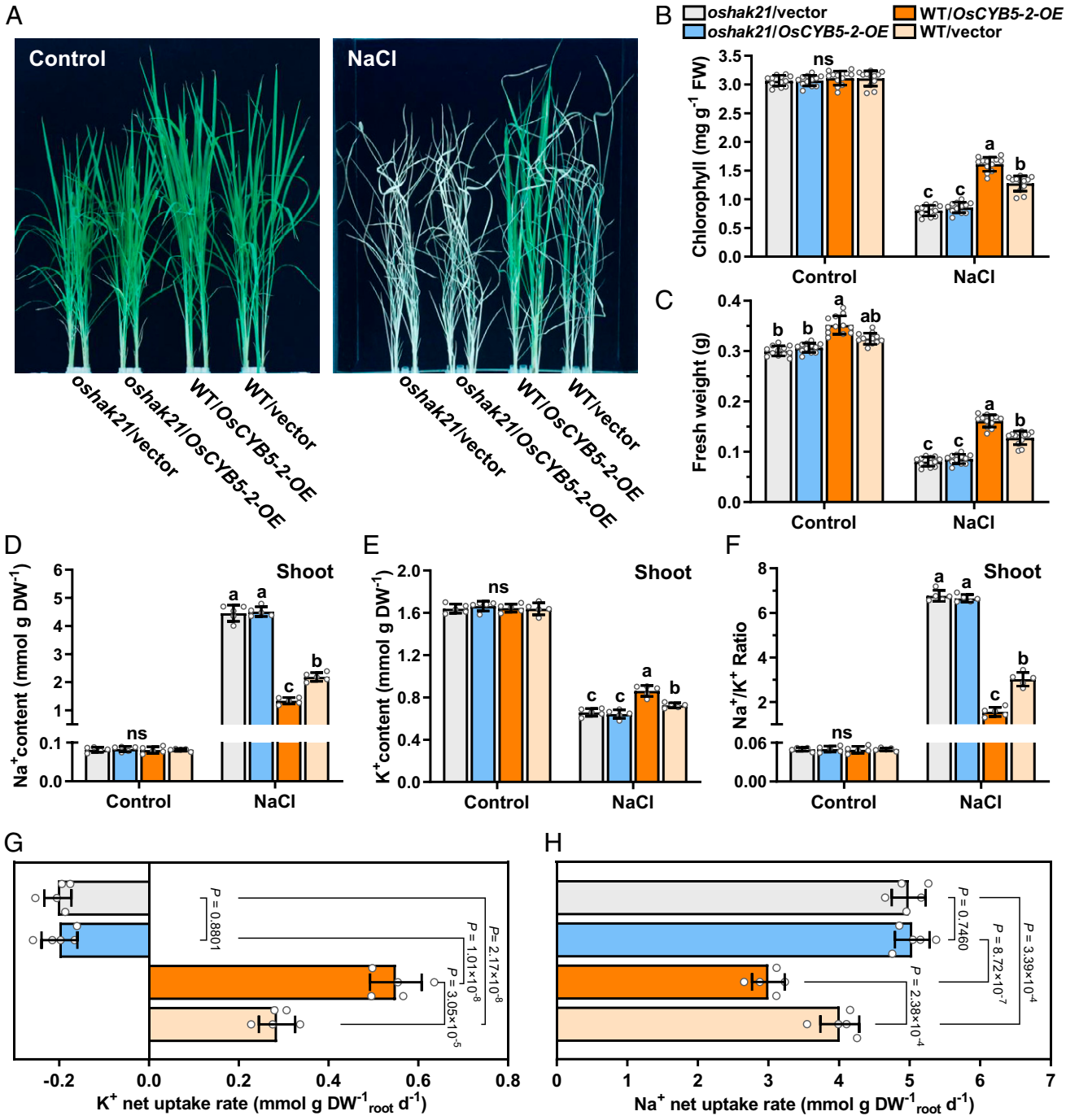

Fig. 3. OsCYB5-2 improves salt tolerance in rice by regulating OsHAK21-mediated K^+ transport. (*A–C*) Phenotypes of *OsCYB5-2*-overexpressed lines in WT (Nipponbare) and *oshak21* backgrounds. Rice seedlings were hydroponically grown with or without 150 mM NaCl for 12 d. Representative photographs of plants (*A*), total chlorophyll in shoots (*B*), and fresh weight (*C*) are shown. The transformed empty vector (pCM1307) seedlings were used as negative controls. (*D–F*) Effects of *OsCYB5-2*-overexpression on Na^+ and K^+ accumulation in shoots under salt stress. Seedlings were treated as in *A*, and the shoots were harvested for Na^+ and K^+ content assay. DW, dry weight. Data are shown as means ± SD (*B* and *C*, $n = 12$; *D–F*, $n = 5$ biologically independent seedlings for each transgenic rice lines). Lowercase letters above the bars in *B–F* indicate significant differences among means (P value = 0.05, Kruskal–Wallis bilateral test). ns indicates nonsubstantial differences at that level of significance. (*G* and *H*) K^+ and Na^+ net uptake rates in rice seedlings during 10 d of the treatment with 150 mM NaCl. Data in *G* and *H* are shown as means ± SD ($n = 5$). Statistically significant differences were determined by the two-tailed Student's *t* test.

constructed and tested in the yeast split-ubiquitin system (Fig. 5*A*). The cytoplasmic C-terminal fragment of OsHAK21 did not bind OsCYB5-2 (Fig. 5*A*). The C-terminal deletions up to 183–amino acid (aa) residues did not significantly affect OsCYB5-2 binding (Fig. 5*A*), suggesting that the OsCYB5-2 binding domain resides within the first 183-aa residues. To establish the essential residues for OsCYB5-2 binding within the first 183 residues, site mutations were made. In yeast systems, leucine (L) residues are thought to be essential for the binding of sugar (and sorbitol) transport proteins with MdCYB5 from apple plants (29). We therefore performed site-directed mutagenesis to separately replace each of the 10 L residues (within

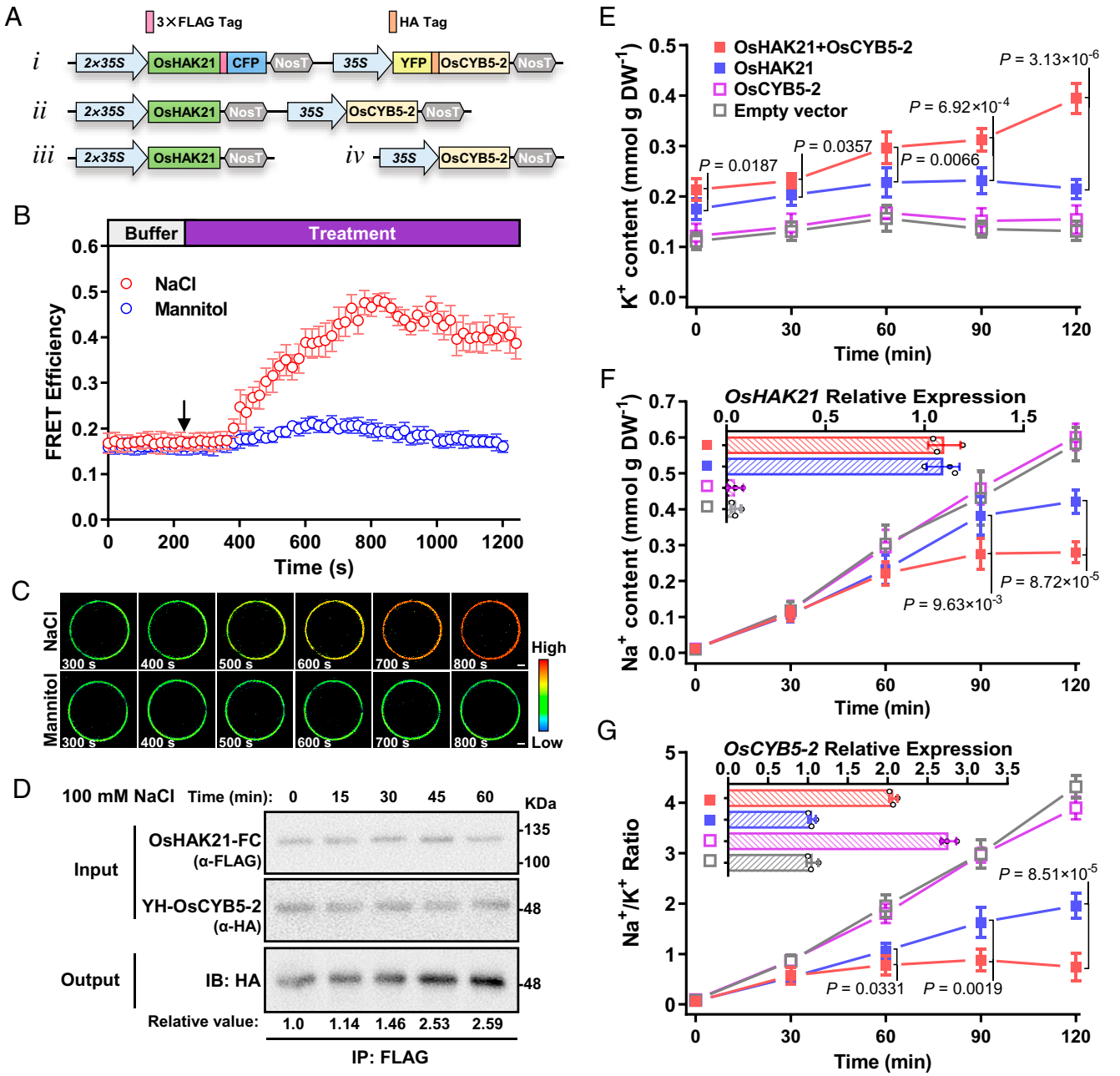

Fig. 4. The interaction between OsHAK21 and OsCYB5-2 is triggered by salt treatment. (*A*) Schematic diagram of the coexpression proteins integrated into a vector. The vectors (*i* and *ii*) feature two independent expression cassettes with two strong promoters (2×*35S* and *35S* promoter) for high-level expression in plant cells. The vector (*i*) encoding CFP and YFP fusion proteins also encoded an in-frame 3×FLAG and HA tag as indicated and consequently were dual-use for FRET (*B* and *C*) and co-IP assays (*D*). Proteins coexpressed from *ii* without fusion tag were used to detect the function of ion transport (*E*–*G*). *iii* and *iv* were used as controls for protein expression alone. NosT, terminator of the *Nos* gene. (*B*) The FRET efficiency (FRET/CFP) of the interaction triggered by 100 mM NaCl and 200 mM mannitol in protoplasts coexpressing OsHAK21-FC+YH-OsCYB5-2 (*i* in *A*). FC, FLAG-CFP Tag; YH, YFP-HA Tag. The arrow indicates the addition of treatments. The data represent means ± SD from the determination of $n = 10$ rice protoplasts for each treatment. Three independent experiments were repeated with similar results. (*C*) Representative FRET images of cells from *B*. (Scale bar, 20 μm.) (*D*) Time-lapse co-IP assay of the interaction between OsHAK21-FC and YH-OsCYB5-2 (*i* in *A*) in *oshak21* suspension cells treated with 100 mM NaCl. The same quality of proteins (5 mg) from different time points were immunoprecipitated with anti-FLAG beads (IP: FLAG) and detected with anti-HA antibody (IB: HA). The experiment was performed independently three times, and representative results are shown. Bands relative values were determined by ImageJ software. The relative protein level at each time point was normalized to OsHAK21-FC of input, and the value at 0 min was set as standard 1. (*E*–*G*) Time-course accumulation of K^+ content (*E*), Na^+ content (*F*), and Na^+/K^+ ratio (*G*) in *oshak21* suspension cells expressing protein combinations (*ii* through *iv* in *A*) with 100 mM NaCl treatments in the presence of 1 mM KCl. *Insets* show the transcripts of *OsHAK21* (*F*) and *OsCYB5-2* (*G*) in independent *oshak21* suspension cells expressing protein combinations as indicated with different colors in *E*. The data are shown as means ± SD from $n = 5$ biologically suspension cells lines for each protein combination. Statistically significant differences were determined by the two-tailed Student's *t* test. Three independent experiments were done with similar results.

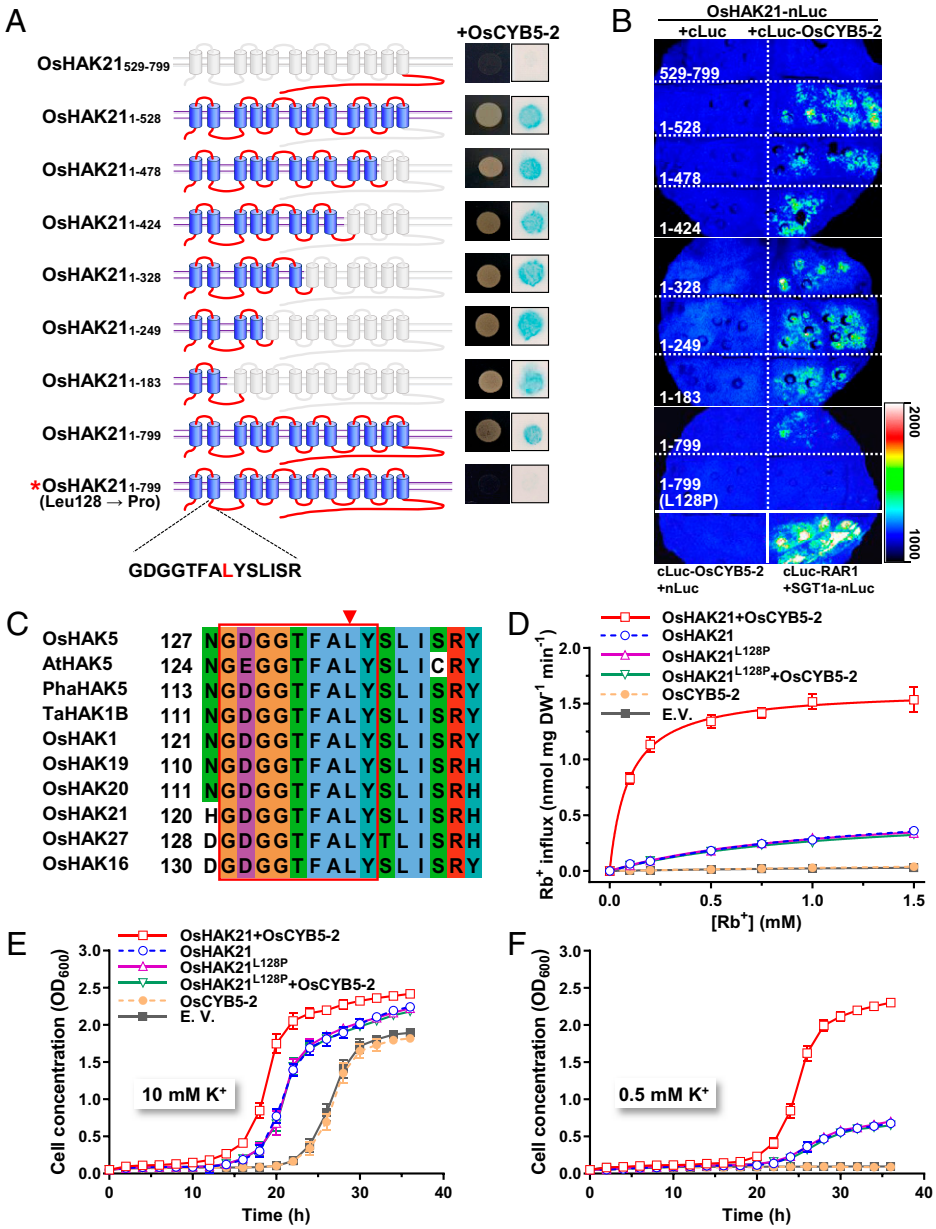

Fig. 5. OsCYB5-2 interacts with OsHAK21 at L128. (*A*) The interaction of different OsHAK21 truncations and OsCYB5-2. In the schematic structures of OsHAK21 (*Left*), the gray portions indicate the sequences removed. The asterisk indicates OsHAK21 with the point mutation at L128P. The *Right* panels indicate the interaction of OsCYB5-2 and different OsHAK21 truncations in yeast split-ubiquitin system (selective medium and β-gal activity test). (*B*) LCI reveals the interaction between different portions of OsHAK21-nLuc and cLuc-OsCYB5-2 in tobacco leaves. The cLuc-RAR1+SGT1a-nLuc was used as a positive control. cLuc: C terminus of luciferase; nLuc: N terminus of luciferase. (*C*) The L128 residue locates between the second and the third transmembrane domains in a highly conserved region (GE/DGGTFALY) among HAK transporters (red box). Arrowhead indicates that the L128 residue of OsHAK21 is conserved in HAK families of different species. (*D*) Initial rates of Rb^+ uptake in yeast R5421 strain expressing different gene combinations. Curves represent results of fitting Michaelis–Menten equation. K_m and V_{max} values are shown in *SI Appendix*, Fig. S11*F*. DW, dry weight. Three independent experiments were carried out, and the data represent the mean ± SD from $n = 3$ biologically independent yeast lines for each genotype. (*E* and *F*) Growth curves of the R5421 strain transformed with OsHAK21 and mutational OsHAK21 with OsCYB5-2 in liquid AP medium supplemented with 10 mM K^+ (*E*) and 0.5 mM K^+ (*F*). Note that the curves of OsHAK21, OsHAK21^{L128P}, and OsHAK21^{L128P}+OsCYB5-2 almost overlap in *D*–*F*.

the identified 1- to 183-aa fragment) with proline (P) in full-length OsHAK21. Finally, the L128P mutation, which lies in the intracellular loop region between transmembrane regions 2 and 3, disrupted OsCYB5-2 binding (Fig. 5*A* and *SI Appendix*, Fig. S11 *A* and *B*). The L128P mutation did not change the expression or PM localization of OsHAK21 (*SI Appendix*, Fig. S11 *C*–*G*). Mutation of other L residues did not significantly influence OsCYB5-2/OsHAK21 binding (*SI Appendix*, Fig. S11 *A* and *B*). The assay was repeated in tobacco leaves using luciferase complementation imaging (LCI) and co-IP (Fig. 5*B* and *SI Appendix*, Fig. S11*E*), which confirmed the yeast split-ubiquitin results. It is worth noting that L128 of OsHAK21 is conserved among representative HAK family members in different plant species (Fig. 5*C*).

To further reveal the role of OsCYB5-2 binding in K^+ transport mediated by OsHAK21, a kinetic characterization of Rb^+ (K^+) transport was performed in yeast cells. Coexpression of OsCYB5-2 together with OsHAK21 increased the affinity for

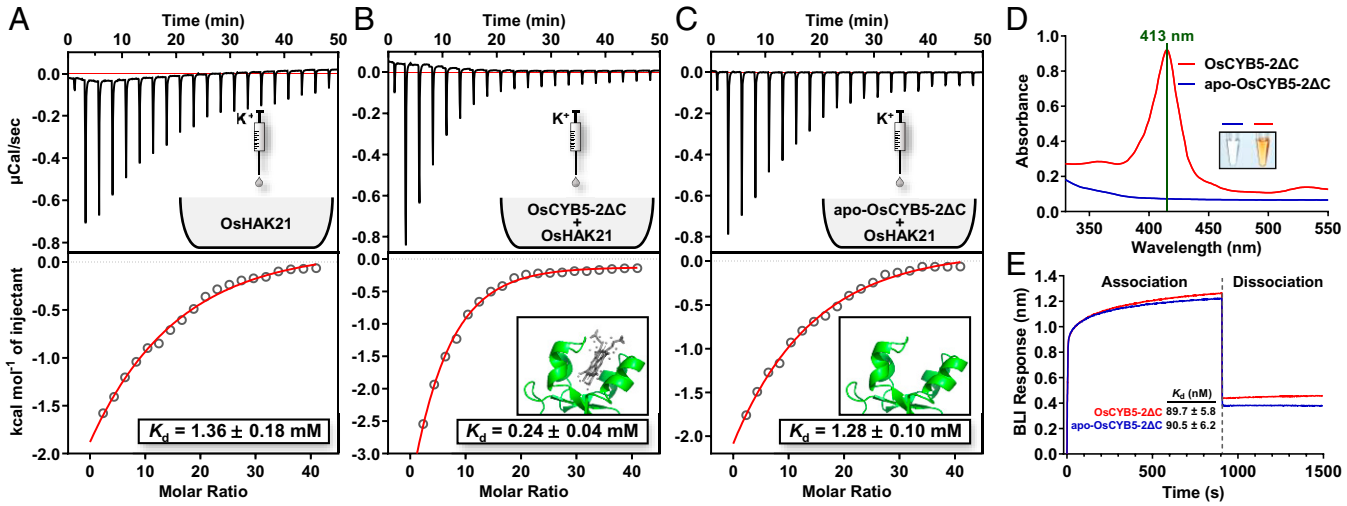

Fig. 6. OsCYB5-2 increases the apparent affinity of OsHAK21 for K^+-binding. (*A–C*) ITC profiles and thermodynamic data of OsHAK21 (*A*), OsHAK21+OsCYB5-2ΔC (*B*), and OsHAK21+apo-OsCYB5-2ΔC (*C*) titrated with K^+. In total, 19 injections of KCl solution were added to protein solution in ITC chamber. During each injection, a small amount of KCl is rapidly mixed with the protein, from which heat is exchanged and recorded in the resulting thermogram. The area of each injection peak (*Top* of *A–C*) is equal to the heat released from that injection with time. The complete binding isotherm for K^+–protein interaction (*Bottom* of *A–C*) was obtained by integrated heat plotted against the molar ratio (ligand/protein) injection of K^+ to protein in ITC chamber. The calculated curve (hollow red line of *Bottom* panel) was fitted by single ion-binding model to obtain the apparent K_d. In addition, the *Insets* in the *Bottom* panel of *B* and *C* show the homologous structure of OsCYB5-2 with heme and apo-OsCYB5-2 without heme, respectively, based on microsomal rabbit CYB5 (Protein Data Bank identifier 2M33). (*D*) Ultraviolet-visible spectra indicate a Soret peak for OsCYB5-2ΔC but not for apo-OsCYB5-2ΔC. *Inset* shows the purified proteins of OsCYB5-2ΔC and apo-OsCYB5-2ΔC. (*E*) Biolayer interferometry (BLI) analysis for the interactions between OsHAK21 and OsCYB5-2ΔC and OsHAK21 and apo-OsCYB5-2ΔC.

Rb^+ (K_m) and maximal rate of uptake (V_{max}) 12- and 2.6-fold, respectively, compared to OsHAK21 alone (Fig. 5*D* and *SI Appendix*, Fig. S11*H*). The L128P mutation in OsHAK21 almost abolished the stimulation by OsCYB5-2 (OsHAK21^{L128P}+OsCYB5-2 versus OsHAK21+OsCYB5-2). However, the mutation had no significant effect on the transport activity of OsHAK21 (OsHAK21 versus OsHAK21^{L128P}), both in terms of V_{max} and K_m (Fig. 5*D* and *SI Appendix*, Fig. S11*H*). Quantitative analysis of yeast growth in liquid culture revealed that the expression of OsHAK21 and OsHAK21^{L128P} improved the yeast growth rate at both 10 and 0.5 mM K^+ compared to the empty vector. Coexpression of OsCYB5-2 further improved yeast growth with OsHAK21, but not with OsHAK21^{L128P} (Fig. 5 *E* and *F*). The effect of the combination of OsCYB5-2 and OsHAK21 on yeast growth was more obvious in medium with lower levels of K^+, and the expression of OsCYB5-2 only had no effect (Fig. 5 *E* and *F*). Taken together, the results suggest that the association of OsCYB5-2 with OsHAK21 at L128 could impact K^+-binding, thus regulating OsHAK21-mediated K^+ transport.

OsCYB5-2 Increases Apparent Affinity of OsHAK21 for K^+-binding. To investigate the biochemical mechanisms by which OsCYB52 improves OsHAK21-mediated K^+ transport, we measured the apparent dissociation constant (K_d) of K^+ and OsHAK21 using isothermal titration calorimetry (ITC). As direct binding measurements of transporters and substrates can be difficult because of low substrate affinity and low levels of purified protein (41), we expressed full-length OsHAK21 protein in *Spodoptera frugiperda* 9 insect cells and purified the protein (*SI Appendix*, Fig. S12*A*). ITC was performed by titrating a solution containing KCl into an ITC chamber, with OsHAK21 protein dissolved in buffer with 50 mM NaCl as the background electrolyte for solubilization (Fig. 6 *A*, *Top*). The heat from each injection was used to obtain the apparent K_d of 1.36 mM (Fig. 6 *A*, *Bottom*). When 50 mM lithium chloride (LiCl) was used as the background electrolyte, similar K_d values were recorded (*SI Appendix*, Fig. S13*A*). No released heat was detected when KCl was substituted with NaCl (LiCl as the background electrolyte) (*SI Appendix*, Fig. S13*B*), indicating that K^+, as opposed to Cl^-, binds OsHAK21 and that the binding is K^+ specific.

We next explored the effect of OsCYB5-2 binding on OsHAK21 for K^+ affinity. Due to the technical difficulties associated with studying interactions between two membrane proteins, we expressed the cytoplasmic fraction of OsCYB5-2 (designated OsCYB5-2ΔC), which contains negatively charged residues likely involved in protein binding, and a heme-binding domain likely involved in electron transfer (24, 42–44). Apo-OsCYB5-2ΔC, which contains no bound heme group, was also expressed (*SI Appendix*, Fig. S12 *B* and *C*). The heme-binding OsCYB5-2ΔC protein exhibited a clear Soret peak at 413 nm in ferric iron (Fe^{3+}) solution, whereas apo-OsCYB5-2ΔC did not (Fig. 6*D*). Heme-binding did not affect OsCYB5-2 binding to OsHAK21, according to a biolayer interferometry (BLI) assay (Fig. 6*E* and *SI Appendix*, Fig. S12*C*). The presence of OsCYB5-2ΔC (OsCYB5-2ΔC:OsHAK21 ratio = 1:1) decreased the K_d of OsHAK21 for K^+ approximately sixfold from 1.36 to 0.24 mM (Fig. 6 *A* and *B*). By contrast, apo-OsCYB5-2ΔC did not change the K_d of OsHAK21 for K^+ (Fig. 6*C*). Neither OsCYB5-2ΔC nor apo-OsCYB5-2ΔC bound K^+ directly (*SI Appendix*, Fig. S13 *C* and *D*). The results suggest that heme-bound OsCYB5-2 enhances the apparent affinity of OsHAK21 for K^+-binding.

OsCYB5-2 Reduces OsHAK21 Sensitivity to Na^+. In saline environments, plant cells accumulate high concentrations of Na^+, which prompted us to investigate whether high-salt concentrations affect OsHAK21 affinity for K^+. We measured the apparent K^+ affinity in the presence of different concentrations of NaCl. As seen in Fig. 7*A*, NaCl concentrations (50 to 200 mM) reduced the affinity of OsHAK21 for K^+ by increasing the K_d, and the reduction was dose dependent. As Na^+ does not bind OsHAK21 directly (*SI Appendix*, Fig. S13*B*), the reduction in apparent affinity for K^+ could have been caused by the high

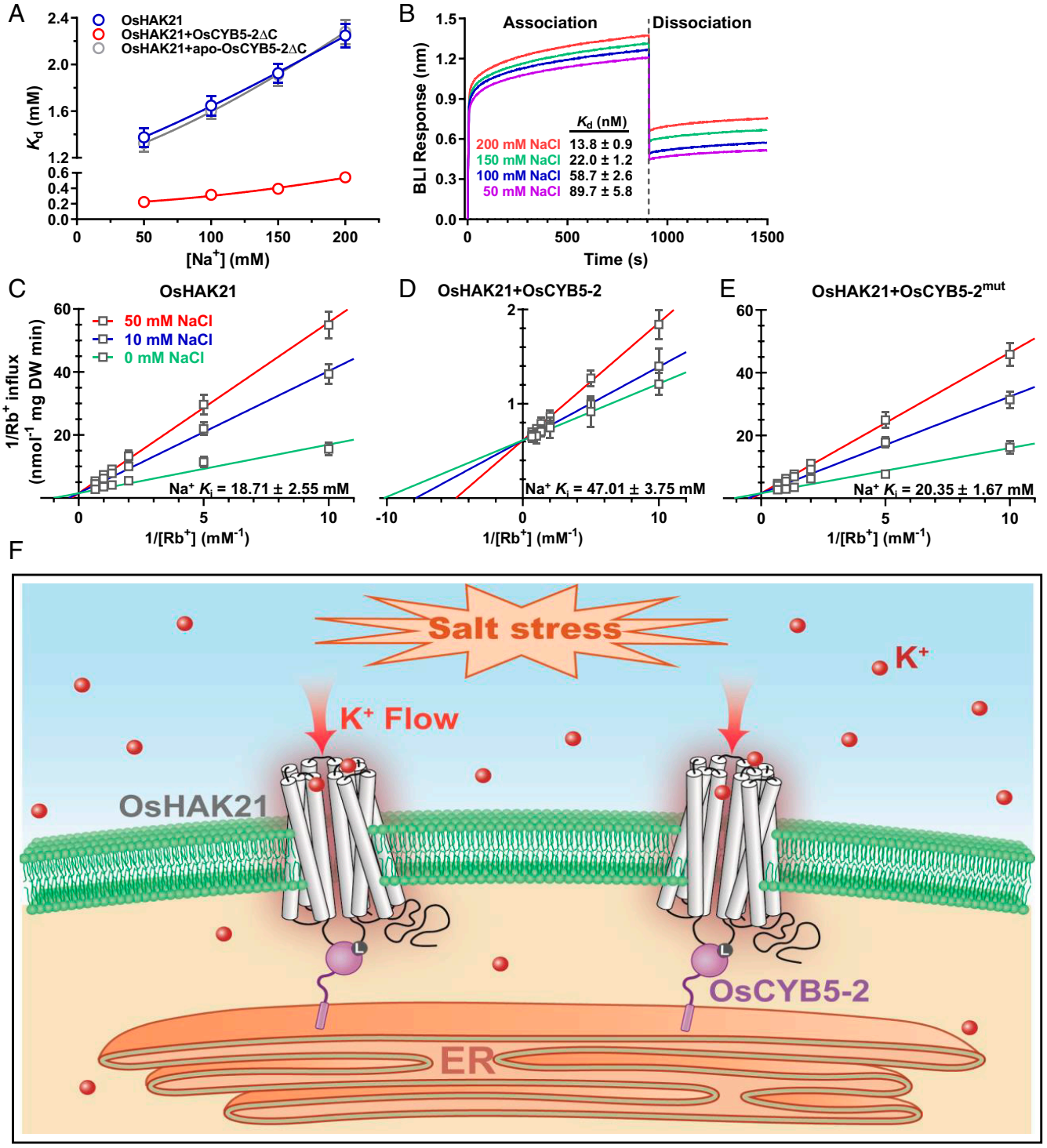

Fig. 7. K^+-binding and transport activity of OsHAK21 are improved by OsCYB5-2 under salt stress. (*A*) Apparent K_d of K^+-binding to OsHAK21, OsHAK21+OsCYB5-2ΔC, and OsHAK21+apo-OsCYB5-2ΔC at different concentrations of Na^+. The data are shown as means ± SD from $n = 3$ independent ITC determination. (*B*) BLI analysis for the interaction between OsHAK21 and OsCYB5-2ΔC at different Na^+ concentrations in solution. (*C–E*) Lineweaver–Burk double-reciprocal plot for Rb^+ uptake in yeast expressing OsHAK21 (*C*), OsHAK21+OsCYB5-2 (*D*), and OsHAK21+OsCYB5-2^{mut} (*E*) in the absence (0 mM) or presence of 10 or 50 mM Na^+. "Na^+ K_i" represents the inhibition constant of Na^+. DW, dry weight. All experiments have been repeated three times, and the data are shown as mean ± SD ($n = 5$). (*F*) Schematic model for OsCYB5-2 and OsHAK21 interaction in salt response. Salt stress enhances ER-localized OsCYB5-2 binding to PM-localized OsHAK21, promoting OsHAK21 affinity and preference for K^+-binding. As a result, OsHAK21-mediated, inward K^+ transport maintains intracellular K^+/Na^+ homeostasis and ultimately improves salt tolerance in rice.

ionic strength of the solution. When OsCYB5-2ΔC was added to the solution, the reduction in OsHAK21 apparent affinity for K^+ was significantly less pronounced at all NaCl concentrations examined (Fig. 7*A*); this effect was not observed with added apo-OsCYB5-2ΔC. Furthermore, NaCl increased the binding affinities between OsHAK21 and OsCYB5-2ΔC, as determined

using BLI methods with biotin-labeled proteins (Fig. 7*B*), consistent with the FRET results (Fig. 4*B*). Importantly, OsHAK21 and OsCYB5-2ΔC bind at a physiologically viable level (nanomolar), suggesting that the binding could occur in plant cells.

To functionally characterize the affinity of OsCYB5-2–OsHAK21 for K^+ under salt treatment, kinetic parameters (inhibition constant K_i for Na^+) were assessed in yeast cells. The $Rb^+(K^+)$-uptake in the presence of Na^+ demonstrated that Na^+ resulted in competitive inhibition, with a K_i of 18.17 mM for $Rb^+(K^+)$-uptake in cells expressing OsHAK21 (Fig. 7*C*). The K_i of Na^+ was increased 2.6-fold by the expression of OsCYB5-2 and OsHAK21 compared to OsHAK21 alone (Fig. 7 *C* and *D*), suggesting that OsCYB5-2 alleviated the inhibitory effect of Na^+ on OsHAK21. The L128P mutation did not obviously change the inhibition of OsHAK21 by Na^+ but abolished the alleviatory effects of OsCYB5-2 on OsHAK21 (Fig. 7*C* and *SI Appendix*, Fig. S11 *I* and *J*).

To explore the effect of the electron carrier properties of OsCYB5-2 on OsHAK21-mediated K^+-uptake, we generated OsCYB5-2^{mut} by substituting two conserved His residues with alanine (H40A/H64A) to impair the coordination with heme iron and the electron transfer properties of OsCYB5-2 (*SI Appendix*, Fig. S14*A*) (24, 26). Like the L128P mutation in OsHAK21, OsCYB5-2^{mut} was unable to stimulate the transport activity of OsHAK21 (*SI Appendix*, Figs. S11*H* and 14*B*) and recovered the inhibitory effect of Na^+ on OsHAK21-mediated $Rb^+(K^+)$-uptake (Fig. 7 *C* and *E*). However, mutation of OsCYB5-2^{mut} did not change its association with OsHAK21 or ER localization (*SI Appendix*, Fig. S14 *C–G*). Taken together, these findings demonstrate that heme-binding and thus the electron transfer properties of OsCYB5-2 are essential for regulating the transport activity of OsHAK21 by improving K^+-binding, especially under NaCl stress.

Discussion

Our understanding of effective quantitative trait loci, genes, and pathways that play roles in the avoidance of Na^+ toxicity at cellular and tissue levels has steadily improved (45–47). Evidence is also increasing regarding the importance of K^+-uptake (via HAKs, AKTs, and HKTs, etc.) and K^+/Na^+ homeostasis under salt stress (4, 47, 48), although no mechanistic insights into salt-related regulation of K^+ transporter have been achieved. In this study, we report a posttranslational mechanism for the regulation of HAK transporter activity by ER-localized OsCYB5-2. This salt-triggered mechanism counteracts the interference of Na^+ with K^+ high-affinity transport and therefore plays an important role in maintaining K^+/Na^+ homeostasis under salt stress in plants.

Cellular adaptation to stressful environments requires coordinated, interorganellar responses to transduce stress signals and maintain the integrity of cellular structures in both animal and plant cells (49). In a previous study, a functional connection between the PM and microtubules (MTs) was discovered, whereby lipid phosphatidic acid binds to MT-associated protein 65 in response to salt stress (50). More recently, lipid-associated SYT1 contact site expansion in *Arabidopsis* under salt stress was reported, resulting in enhanced ER–PM connectivity (49). However, the role of ER–PM connection in stress adaptation remains unclear. Here, we report that salt stress triggers a rapid ER–PM connection via binding of ER-localized OsCYB5-2 and PM-localized OsHAK21. OsCYB5-2 and OsHAK21 binding and hence ER–PM connection occurred as quickly as 50 s after the onset of NaCl treatment (Fig. 4), which is quicker than that in *Arabidopsis*, in which phosphoinositide-associated SYT1 contact site expansion occurs within hours (49).

OsCYB5-2 and OsHAK21 interaction was not only observed at the protoplast and cellular level (Figs. 1 and 4) but also in whole rice plants. Overexpression of *OsCYB5-2* conferred increased salt tolerance to WT plants but not to *oshak21* mutant plants that lack the partner protein OsHAK21 (Fig. 3), providing further evidence that the OsCYB5-2–OsHAK21 interaction plays a positive role in regulating salt tolerance.

Plant HAK transporters are predicted to contain 10 to 14 transmembrane domains, with both the N and C termini facing the cytoplasm (51). On the N-terminal side, the GD(E)GGTFALY motif is highly conserved among members of the HAK family (Fig. 5*C*) (52). The L128 residue, which is required for OsCYB5-2 binding, is located within the GDGGTFALY motif (Fig. 5). Residue substitution (F130S) in AtHAK5 led to an increase in K^+ affinity by >100-fold in yeast (52). AtHAK5 activity was also found to be regulated by CIPK23/CBL1 complex–mediated phosphorylation of the N-terminal 1- to 95-aa residues (14). In rice, a receptor-like kinase RUPO interacts with the C-tail of OsHAKs to mediate K^+ homeostasis (53). Thus, the L128 bound by OsCYB5 identified in this work is uniquely involved in HAK transporter regulation.

OsCYB5-2 binding at L128 elicits an increase in K^+-uptake (Fig. 5*D*), consistent with the role of OsCYB5-2 in enhancing the apparent affinity of OsHAK21 for K^+-binding (Fig. 6). An important question is raised by this: how does OsCYB5-2 regulate OsHAK21 affinity for K^+? Electron transfer between CYB5 and its redox partners is reliant upon its heme cofactor (24, 42). Given that both apo-OsCYB5-2ΔC (no heme) and OsCYB5-2^{mut} are unable to stimulate K^+ affinity of OsHAK21 (Figs. 6 and 7 and *SI Appendix*, Figs. S14 and S15), we propose that electron transfer is an essential mechanism for OsCYB5-2 function. This could occur via redox modification of OsHAK21 to increase K^+ affinity. We cannot, however, rule out the possibility of allosteric effects of OsCYB5-2 binding on OsHAK21. Several residues in AtHAK5 have been proposed as the sites of K^+-binding or -filtering (20, 54). Following association of OsCYB5-2 with residue L128 of OsHAK21, a conformational change likely occurs in OsHAK21, resulting in a modulated binding efficiency for K^+.

Active transporters and ion channels coordinate to produce and dissipate ionic gradients, allowing cells to control and finely tune their internal ionic composition (55). However, under salt stress, apoplastic Na^+ entry into cells depolarizes the PM, making channel-mediated K^+-uptake thermodynamically impossible. By contrast, activation of the gated, outward-rectifying K^+ channel induces K^+ efflux out of cells. Together, these effects dramatically reduce the K^+ concentration in plant cells. K^+-uptake is therefore dependent on active transport via K^+/H^+ symport mechanisms (HAK family), which are driven by the proton motive force generated by H^+-ATPase (48). A strong, positive correlation between H^+-ATPase activity and salinity stress tolerance has been reported (56, 57). In rice, OsHAK21 is essential for salt tolerance at the seedling and germination stages (8, 17). OsHAK21-mediated K^+-uptake increased with lowering of the external pH (increasing H^+ concentration); this effect was abolished in the presence of the proton ionophore CCCP (*SI Appendix*, Fig. S15*A*), suggesting that OsHAK21 could act as a K^+/H^+ symporter, which depends on the H^+ gradient. OsCYB5-2 stimulation of OsHAK21-mediated K^+-uptake but not OsCYB5-2-OsHAK21 binding was also pH dependent (*SI Appendix*, Fig. S15 *D–F*). Confirmation of synergistic effects of oxidoreduction and H^+ concentration on OsHAK21 activity requires further study. The CYB5-mediated OsHAK21 activation mechanism reported here differs from the posttranslational modifications that occur via phosphorylation by the CBL/CIPK pair (11, 19, 20), which likely relies on salt perception (which triggers calcium signals) (58).

We propose that salt triggers association of ER-localized OsCYB5-2 with PM-localized OsHAK21, causing the OsHAK21 transporter to specifically and effectively capture K^+. As a result,

OsHAK21 transports K^+ inward to maintain intracellular K^+/Na^+ homeostasis, thus improving salt tolerance in rice (Fig. 7*F*).

Materials and Methods

Information on plant materials used, growth conditions, and experimental methods employed in this study is detailed in *SI Appendix*. The methods include the specifics on vector construction and plant transformation, co-IP assay, FRET analysis, subcellular localization, yeast two-hybrid, histochemical staining, gene expression analysis, LCI assay, BLI, plant treatment, and ion content determination. Details of experimental conditions for ITC are provided in *SI Appendix*, Table S1. Primers used in this study are listed in *SI Appendix*, Table S2.

Data Availability. All study data are included in the article and/or *SI Appendix*.

ACKNOWLEDGMENTS. We thank Professor Qi Xie (Institute of Genetics and Developmental Biology, Chinese Academy of Sciences) for providing the dual split-ubiquitin membrane yeast two-hybrid system. We also thank Professors Weihua Wu and Yi Wang (China Agricultural University) for the generous gift of the *athak5* seeds, p416-GPD with p424-GPD vectors, and the yeast strain R5421 with R757. We thank Professor Xiaorong Tao (Nanjing Agricultural University) for providing the baculovirus expression system. The research was supported by National Natural Science Foundation Grants 31770294 and 32171956, the Fundamental Research Funds for the Central Universities to W.Z., and a start-up fund for advanced talents from Nanjing Agricultural University (680-804016) to F.L.

1. T. Horie *et al.*, Two types of HKT transporters with different properties of Na^+ and K^+ transport in *Oryza sativa*. *Plant J.* **27**, 129–138 (2001).
2. S. Shabala, T. A. Cuin, Potassium transport and plant salt tolerance. *Physiol. Plant.* **133**, 651–669 (2008).
3. U. Anschütz, D. Becker, S. Shabala, Going beyond nutrition: Regulation of potassium homoeostasis as a common denominator of plant adaptive responses to environment. *J. Plant Physiol.* **171**, 670–687 (2014).
4. A. M. Ismail, T. Horie, Genomics, physiology, and molecular breeding approaches for improving salt tolerance. *Annu. Rev. Plant Biol.* **68**, 405–434 (2017).
5. T. A. Cuin *et al.*, Assessing the role of root plasma membrane and tonoplast Na^+/H^+ exchangers in salinity tolerance in wheat: In planta quantification methods. *Plant Cell Environ.* **34**, 947–961 (2011).
6. R. Munns, M. Tester, Mechanisms of salinity tolerance. *Annu. Rev. Plant Biol.* **59**, 651–681 (2008).
7. S. J. Roy, S. Negrão, M. Tester, Salt resistant crop plants. *Curr. Opin. Biotechnol.* **26**, 115–124 (2014).
8. Y. Shen *et al.*, The potassium transporter OsHAK21 functions in the maintenance of ion homeostasis and tolerance to salt stress in rice. *Plant Cell Environ.* **38**, 2766–2779 (2015).
9. Y. Wang, W. H. Wu, Regulation of potassium transport and signaling in plants. *Curr. Opin. Plant Biol.* **39**, 123–128 (2017).
10. A. Grabov, Plant KT/KUP/HAK potassium transporters: Single family – Multiple functions. *Ann. Bot.* **99**, 1035–1041 (2007).
11. J. Böhm *et al.*, Understanding the molecular basis of salt sequestration in epidermal bladder cells of *Chenopodium quinoa*. *Curr. Biol.* **28**, 3075–3085.e7 (2018).
12. P. Ragel, N. Raddatz, E. O. Leidi, F. J. Quintero, J. M. Pardo, Regulation of K^+ nutrition in plants. *Front. Plant Sci.* **10**, 281 (2019).
13. M. Gierth, P. Mäser, J. I. Schroeder, The potassium transporter AtHAK5 functions in K^+ deprivation-induced high-affinity K^+ uptake and AKT1 K^+ channel contribution to K^+ uptake kinetics in *Arabidopsis* roots. *Plant Physiol.* **137**, 1105–1114 (2005).
14. P. Ragel *et al.*, The CBL-interacting protein kinase CIPK23 regulates HAK5-mediated high-affinity K^+ uptake in *Arabidopsis* roots. *Plant Physiol.* **169**, 2863–2873 (2015).
15. G. Chen *et al.*, Rice potassium transporter OsHAK1 is essential for maintaining potassium-mediated growth and functions in salt tolerance over low and high potassium concentration ranges. *Plant Cell Environ.* **38**, 2747–2765 (2015).
16. H. Feng *et al.*, Rice OsHAK16 functions in potassium uptake and translocation in shoot, maintaining potassium homeostasis and salt tolerance. *Planta* **250**, 549–561 (2019).
17. Y. He *et al.*, A quantitative trait locus, *qSE3*, promotes seed germination and seedling establishment under salinity stress in rice. *Plant J.* **97**, 1089–1104 (2019).
18. T. Yang *et al.*, The role of a potassium transporter OsHAK5 in potassium acquisition and transport from roots to shoots in rice at low potassium supply levels. *Plant Physiol.* **166**, 945–959 (2014).
19. S. Scherzer *et al.*, Calcium sensor kinase activates potassium uptake systems in gland cells of Venus flytraps. *Proc. Natl. Acad. Sci. U.S.A.* **112**, 7309–7314 (2015).
20. R. Ródenas *et al.*, Insights into the mechanisms of transport and regulation of the *Arabidopsis* high-affinity K^+ transporter HAK5[1]. *Plant Physiol.* **185**, 1860–1874 (2021).
21. Y. T. Hwang *et al.*, Novel targeting signals mediate the sorting of different isoforms of the tail-anchored membrane protein cytochrome b_5 to either endoplasmic reticulum or mitochondria. *Plant Cell* **16**, 3002–3019 (2004).
22. C. Maggio, A. Barbante, F. Ferro, L. Frigerio, E. Pedrazzini, Intracellular sorting of the tail-anchored protein cytochrome b_5 in plants: A comparative study using different isoforms from rabbit and *Arabidopsis*. *J. Exp. Bot.* **58**, 1365–1379 (2007).
23. T. D. Porter, The roles of cytochrome b_5 in cytochrome P450 reactions. *J. Biochem. Mol. Toxicol.* **16**, 311–316 (2002).
24. J. B. Schenkman, I. Jansson, The many roles of cytochrome b_5. *Pharmacol. Ther.* **97**, 139–152 (2003).
25. A. Bernard *et al.*, Reconstitution of plant alkane biosynthesis in yeast demonstrates that *Arabidopsis* ECERIFERUM1 and ECERIFERUM3 are core components of a very-long-chain alkane synthesis complex. *Plant Cell* **24**, 3106–3118 (2012).
26. M. Gou *et al.*, Cytochrome b_5 is an obligate electron shuttle protein for syringyl lignin biosynthesis in *Arabidopsis*. *Plant Cell* **31**, 1344–1366 (2019).
27. M. Nagano *et al.*, Functional association of cell death suppressor, *Arabidopsis* Bax inhibitor-1, with fatty acid 2-hydroxylation through cytochrome b_5. *Plant J.* **58**, 122–134 (2009).
28. J. Chang, J. M. Clay, C. Chang, Association of cytochrome b_5 with ETR1 ethylene receptor signaling through RTE1 in *Arabidopsis*. *Plant J.* **77**, 558–567 (2014).
29. R. C. Fan *et al.*, Apple sucrose transporter SUT1 and sorbitol transporter SOT6 interact with cytochrome *b*5 to regulate their affinity for substrate sugars. *Plant Physiol.* **150**, 1880–1901 (2009).
30. Y. Li *et al.*, *Arabidopsis* sucrose transporter SUT4 interacts with cytochrome *b*5-2 to regulate seed germination in response to sucrose and glucose. *Mol. Plant* **5**, 1029–1041 (2012).
31. N. Johnsson, A. Varshavsky, Split ubiquitin as a sensor of protein interactions in vivo. *Proc. Natl. Acad. Sci. U.S.A.* **91**, 10340–10344 (1994).
32. R. F. Gaber, C. A. Styles, G. R. Fink, TRK1 encodes a plasma membrane protein required for high-affinity potassium transport in *Saccharomyces cerevisiae*. *Mol. Cell. Biol.* **8**, 2848–2859 (1988).
33. R. L. Nakamura, J. A. Anderson, R. F. Gaber, Determination of key structural requirements of a K^+ channel pore. *J. Biol. Chem.* **272**, 1011–1018 (1997).
34. J. A. Anderson, S. S. Huprikar, L. V. Kochian, W. J. Lucas, R. F. Gaber, Functional expression of a probable *Arabidopsis thaliana* potassium channel in *Saccharomyces cerevisiae*. *Proc. Natl. Acad. Sci. U.S.A.* **89**, 3736–3740 (1992).
35. Y. J. Pyo, M. Gierth, J. I. Schroeder, M. H. Cho, High-affinity K^+ transport in *Arabidopsis*: AtHAK5 and AKT1 are vital for seedling establishment and postgermination growth under low-potassium conditions. *Plant Physiol.* **153**, 863–875 (2010).
36. G. Zhong, Q. Zhu, Y. Li, Y. Liu, H. Wang, Once for all: A novel robust system for co-expression of multiple chimeric fluorescent fusion proteins in plants. *Front, Plant Sci*, **8**, 1071 (2017).
37. W. Li *et al.*, Tissue-specific accumulation of pH-sensing phosphatidic acid determines plant stress tolerance. *Nat. Plants* **5**, 1012–1021 (2019).
38. C. M. Ho, T. Paciorek, E. Abrash, D. C. Bergmann, Modulators of stomatal lineage signal transduction alter membrane contact sites and reveal specialization among ERECTA kinases. *Dev. Cell* **38**, 345–357 (2016).
39. B. Li *et al.*, The receptor-like kinase NIK1 targets FLS2/BAK1 immune complex and inversely modulates antiviral and antibacterial immunity. *Nat. Commun.* **10**, 4996 (2019).
40. D. Lu *et al.*, A receptor-like cytoplasmic kinase, BIK1, associates with a flagellin receptor complex to initiate plant innate immunity. *Proc. Natl. Acad. Sci. U.S.A.* **107**, 496–501 (2010).
41. A. Picollo, M. Malvezzi, J. C. D. Houtman, A. Accardi, Basis of substrate binding and conservation of selectivity in the CLC family of channels and transporters. *Nat. Struct. Mol. Biol.* **16**, 1294–1301 (2009).
42. D. F. Estrada, J. S. Laurence, E. E. Scott, Substrate-modulated cytochrome P450 17A1 and cytochrome b_5 interactions revealed by NMR. *J. Biol. Chem.* **288**, 17008–17018 (2013).
43. S. C. Im, L. Waskell, The interaction of microsomal cytochrome P450 2B4 with its redox partners, cytochrome P450 reductase and cytochrome b_5. *Arch. Biochem. Biophys.* **507**, 144–153 (2011).
44. J. Wu *et al.*, Crystal structure of recombinant trypsin-solubilized fragment of cytochrome b_5 and the structural comparison with Val61His mutant. *Proteins* **40**, 249–257 (2000).
45. Y. Yang, Y. Guo, Elucidating the molecular mechanisms mediating plant salt-stress responses. *New Phytol.* **217**, 523–539 (2018).
46. J. K. Zhu, Abiotic stress signaling and responses in plants. *Cell* **167**, 313–324 (2016).
47. E. van Zelm, Y. Zhang, C. Testerink, Salt tolerance mechanisms of plants. *Annu. Rev. Plant Biol.* **71**, 403–433 (2020).
48. F. Rubio, M. Nieves-Cordones, T. Horie, S. Shabala, Doing 'business as usual' comes with a cost: Evaluating energy cost of maintaining plant intracellular K^+ homeostasis under saline conditions. *New Phytol.* **225**, 1097–1104 (2020).
49. E. Lee *et al.*, Ionic stress enhances ER-PM connectivity via phosphoinositide-associated SYT1 contact site expansion in *Arabidopsis*. *Proc. Natl. Acad. Sci. U.S.A.* **116**, 1420–1429 (2019).
50. Q. Zhang *et al.*, Phosphatidic acid regulates microtubule organization by interacting with MAP65-1 in response to salt stress in *Arabidopsis*. *Plant Cell* **24**, 4555–4576 (2012).
51. M. Gierth, P. Mäser, Potassium transporters in plants–involvement in K^+ acquisition, redistribution and homeostasis. *FEBS Lett.* **581**, 2348–2356 (2007).
52. F. Alemán *et al.*, The F130S point mutation in the *Arabidopsis* high-affinity K^+ transporter AtHAK5 increases K^+ over Na^+ and Cs^+ selectivity and confers Na^+ and Cs^+ tolerance to yeast under heterologous expression. *Front, Plant Sci.* **5**, 430 (2014).

53. L. Liu *et al.*, Receptor-like kinase RUPO interacts with potassium transporters to regulate pollen tube growth and integrity in rice. *PLoS Genet.* **12**, e1006085 (2016).
54. I. Tascón *et al.*, Structural basis of proton-coupled potassium transport in the KUP family. *Nat. Commun.* **11**, 626 (2020).
55. A. Picollo, Y. Xu, N. Johner, S. Bernèche, A. Accardi, Synergistic substrate binding determines the stoichiometry of transport of a prokaryotic H^+/Cl exchanger. *Nat. Struct. Mol. Biol.* **19**, 525–531 (2012).
56. J. Bose *et al.*, Rapid regulation of the plasma membrane H^+-ATPase activity is essential to salinity tolerance in two halophyte species, *Atriplex lentiformis* and *Chenopodium quinoa*. *Ann. Bot.* **115**, 481–494 (2015).
57. L. Shabala *et al.*, Cell-type-specific H^+-ATPase activity in root tissues enables K^+ retention and mediates acclimation of barley (*Hordeum vulgare*) to salinity stress. *Plant Physiol.* **172**, 2445–2458 (2016).
58. Z. Jiang *et al.*, Plant cell-surface GIPC sphingolipids sense salt to trigger Ca^{2+} influx. *Nature* **572**, 341–346 (2019).